



HAL
open science

Introducing global peat-specific temperature and pH calibrations based on brGDGT bacterial lipids

A. Naafs, G.N. Inglis, Y. Zheng, J. Amesbury, H. Biester, R. Bindler, J. Blewett, A. Burrows, D. del Castillo Torres, F. Chambers, et al.

► To cite this version:

A. Naafs, G.N. Inglis, Y. Zheng, J. Amesbury, H. Biester, et al.. Introducing global peat-specific temperature and pH calibrations based on brGDGT bacterial lipids. *Geochimica et Cosmochimica Acta*, 2017, 208, pp.285-301. 10.1016/j.gca.2017.01.038 . insu-01474123

HAL Id: insu-01474123

<https://insu.hal.science/insu-01474123v1>

Submitted on 22 Feb 2017

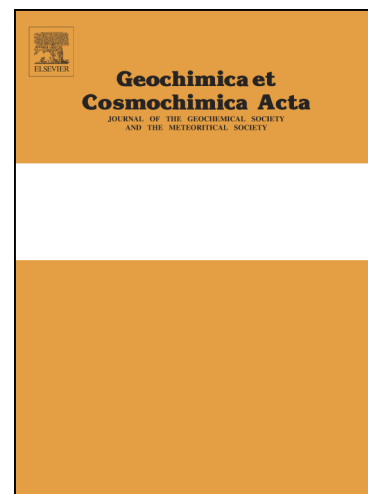
HAL is a multi-disciplinary open access archive for the deposit and dissemination of scientific research documents, whether they are published or not. The documents may come from teaching and research institutions in France or abroad, or from public or private research centers.

L'archive ouverte pluridisciplinaire **HAL**, est destinée au dépôt et à la diffusion de documents scientifiques de niveau recherche, publiés ou non, émanant des établissements d'enseignement et de recherche français ou étrangers, des laboratoires publics ou privés.



Distributed under a Creative Commons Attribution - NonCommercial - NoDerivatives 4.0 International License

Accepted Manuscript



Introducing global peat-specific temperature and pH calibrations based on brGDGT bacterial lipids

B.D.A. Naafs, G.N. Inglis, Y. Zheng, M.J. Amesbury, H. Biester, R. Bindler, J. Blewett, M.A. Burrows, D. del Castillo Torres, F.M. Chambers, A.D. Cohen, R.P. Evershed, S.J. Feakins, A. Gallego-Sala, L. Gandois, D.M. Gray, P.G. Hatcher, E.N. Honorio Coronado, P.D.M. Hughes, A. Huguet, M. Könönen, F. Laggoun-Défarge, O. Lähteenoja, R. Marchant, E. McClymont, X. Pontevedra-Pombal, C. Ponton, A. Pourmand, A.M. Rizzuti, L. Rochefort, J. Schellekens, F. De Vleeschouwer, R.D. Pancost

PII: S0016-7037(17)30052-2
DOI: <http://dx.doi.org/10.1016/j.gca.2017.01.038>
Reference: GCA 10132

To appear in: *Geochimica et Cosmochimica Acta*

Received Date: 2 June 2016
Revised Date: 14 January 2017
Accepted Date: 18 January 2017

Please cite this article as: Naafs, B.D.A., Inglis, G.N., Zheng, Y., Amesbury, M.J., Biester, H., Bindler, R., Blewett, J., Burrows, M.A., del Castillo Torres, D., Chambers, F.M., Cohen, A.D., Evershed, R.P., Feakins, S.J., Gallego-Sala, A., Gandois, L., Gray, D.M., Hatcher, P.G., Honorio Coronado, E.N., Hughes, P.D.M., Huguet, A., Könönen, M., Laggoun-Défarge, F., Lähteenoja, O., Marchant, R., McClymont, E., Pontevedra-Pombal, X., Ponton, C., Pourmand, A., Rizzuti, A.M., Rochefort, L., Schellekens, J., De Vleeschouwer, F., Pancost, R.D., Introducing global peat-specific temperature and pH calibrations based on brGDGT bacterial lipids, *Geochimica et Cosmochimica Acta* (2017), doi: <http://dx.doi.org/10.1016/j.gca.2017.01.038>

This is a PDF file of an unedited manuscript that has been accepted for publication. As a service to our customers we are providing this early version of the manuscript. The manuscript will undergo copyediting, typesetting, and review of the resulting proof before it is published in its final form. Please note that during the production process errors may be discovered which could affect the content, and all legal disclaimers that apply to the journal pertain.

1 **Introducing global peat-specific temperature and pH calibrations based on**
2 **brGDGT bacterial lipids**

3
4 B.D.A. Naafs^{1,2*}, G.N. Inglis^{1,2}, Y. Zheng³, M.J. Amesbury⁴, H. Biester⁵, R. Bindler⁶,
5 J. Blewett^{1,2}, M.A. Burrows⁷, D. del Castillo Torres⁸, F.M. Chambers⁹, A.D. Cohen¹⁰,
6 R.P. Evershed^{1,2}, S.J. Feakins¹¹, A. Gallego-Sala⁴, L. Gandois¹², D.M. Gray¹³, P.G.
7 Hatcher¹⁴, E.N. Honorio Coronado⁸, P.D.M. Hughes¹⁵, A. Huguet¹⁶, M. Könönen¹⁷, F.
8 Laggoun-Défarge¹⁸, O. Läähteenoja¹⁹, R. Marchant²⁰, E. McClymont^{1,21}, X.
9 Pontevedra-Pombal²², C. Ponton¹¹, A. Pourmand²³, A.M. Rizzuti²⁴, L. Rochefort²⁵, J.
10 Schellekens²⁶, F. De Vleeschouwer¹², and R.D. Pancost^{1,2}

11
12 ¹Organic Geochemistry Unit, School of Chemistry, University of Bristol, Bristol, UK

13 ²Cabot Institute, University of Bristol, Bristol, UK

14 ³State Key Laboratory of Continental Dynamics, Department of Geology, Northwest
15 University, Xi'an, PR China

16 ⁴Geography, College of Life and Environmental Sciences, University of Exeter,
17 Exeter, UK

18 ⁵Institut für Geoökologie, AG Umweltgeochemie, Technische Universität
19 Braunschweig, Braunschweig, Germany

20 ⁶Department of Ecology and Environmental Science, Umeå University, Umeå,
21 Sweden

22 ⁷Australian National University, Acton, Canberra, Australia

23 ⁸Instituto de Investigaciones de la Amazonía Peruana (IIAP), Iquitos, Perú

24 ⁹Centre for Environmental Change and Quaternary Research, School of Natural and
25 Social Sciences, University of Gloucestershire, Cheltenham, UK

26 ¹⁰Department of Earth and Ocean Sciences, University of South Carolina, Columbia,
27 USA

28 ¹¹Department of Earth Sciences, University of Southern California, Los Angeles,
29 USA

30 ¹²ECOLAB, Université de Toulouse, CNRS, INPT, UPS, Toulouse, France

31 ¹³Pinelands Field Station, Rutgers University, New Lisbon, USA

32 ¹⁴Department of Chemistry and Biochemistry, Old Dominion University, Norfolk,
33 USA

34 ¹⁵Palaeoecology Laboratory, University of Southampton, Southampton, UK

- 35 ¹⁶Sorbonne Universités, UPMC, Univ Paris 06, CNRS, EPHE, UMR 7619 METIS,
 36 Paris, France
- 37 ¹⁷Department of Forest Sciences, University of Helsinki, Finland
- 38 ¹⁸Université d'Orléans / CNRS /BRGM, ISTO, UMR 7327, Orléans, France
- 39 ¹⁹Department of Biology, University of Turku, Finland
- 40 ²⁰York Institute for Tropical Ecosystems, Environment Department, Wentworth Way
 41 University of York, York, UK
- 42 ²¹Department of Geography, Durham University, Durham, UK
- 43 ²²Departamento de Edafología e Química Agrícola, Universidade de Santiago de
 44 Compostela, Santiago de Compostela, Spain
- 45 ²³Division of Marine Geology & Geophysics, University of Miami – RSMAS, Miami,
 46 USA
- 47 ²⁴Department of Chemistry, Claflin University, Orangeburg, USA
- 48 ²⁵Peatland Ecology Research Group (PERG), Centre for Northern Studies, Université
 49 Laval, Quebec City, Canada
- 50 ²⁶Department of Soil Science, University of São Paulo, Piracicaba, Brazil

51

52 *Corresponding author (david.naafs@bristol.ac.uk)

53

54 **Abstract**

55 Glycerol dialkyl glycerol tetraethers (GDGTs) are membrane-spanning lipids from
 56 Bacteria and Archaea that are ubiquitous in a range of natural archives and especially
 57 abundant in peat. Previous work demonstrated that the distribution of bacterial
 58 branched GDGTs (brGDGTs) in mineral soils is correlated to environmental factors
 59 such as mean annual air temperature (MAAT) and soil pH. However, the influence of
 60 these parameters on brGDGT distributions in peat is largely unknown. Here we
 61 investigate the distribution of brGDGTs in 470 samples from 96 peatlands around the
 62 world with a broad mean annual air temperature (−8 to 27 °C) and pH (3–8) range and
 63 present the first peat-specific brGDGT-based temperature and pH calibrations. Our
 64 results demonstrate that the degree of cyclisation of brGDGTs in peat is positively
 65 correlated with pH, $\text{pH} = 2.49 \times \text{CBT}_{\text{peat}} + 8.07$ ($n = 51$, $R^2 = 0.58$, $\text{RMSE} = 0.8$) and
 66 the degree of methylation of brGDGTs is positively correlated with MAAT,
 67 $\text{MAAT}_{\text{peat}} (\text{°C}) = 52.18 \times \text{MBT}_{5\text{me}}' - 23.05$ ($n = 96$, $R^2 = 0.76$, $\text{RMSE} = 4.7 \text{ °C}$).

68 These peat-specific calibrations are distinct from the available mineral soil
69 calibrations. In light of the error in the temperature calibration (~ 4.7 °C), we urge
70 caution in any application to reconstruct late Holocene climate variability, where the
71 climatic signals are relatively small, and the duration of excursions could be brief.
72 Instead, these proxies are well-suited to reconstruct large amplitude, longer-term
73 shifts in climate such as deglacial transitions. Indeed, when applied to a peat deposit
74 spanning the late glacial period (~ 15.2 kyr), we demonstrate that $MAAT_{\text{peat}}$ yields
75 absolute temperatures and relative temperature changes that are consistent with those
76 from other proxies. In addition, the application of $MAAT_{\text{peat}}$ to fossil peat (i.e.
77 lignites) has the potential to reconstruct terrestrial climate during the Cenozoic. We
78 conclude that there is clear potential to use brGDGTs in peats and lignites to
79 reconstruct past terrestrial climate.

80

81 *Keyword: GDGT, biomarker, peatland, calibration, lignite*

82

83 Highlights:

- 84 - Analysis of brGDGT distributions in global peat dataset
- 85 - Correlation of brGDGT distributions with peat pH and mean annual air temperature
- 86 - Development of peat-specific temperature and pH proxies

87 1. Introduction

88 Although reconstructions of terrestrial environments are crucial for the understanding
89 of Earth's climate system, suitable depositional archives (especially longer continuous
90 sequences) are rare on land. Peatlands and lignites (naturally compressed ancient peat)
91 are one exception and offer remarkable preservation of organic matter. Peats can be
92 found in all climate zones where suitable waterlogged conditions exist. Typical peat
93 accumulation rates are on the order of 1-2 mm/year (Gorham et al., 2003) and because
94 they exhibit minimal bioturbation (although roots might be present) they are widely
95 used as climate archives during the late Quaternary, predominantly the Holocene
96 (e.g., Barber, 1993; Chambers and Charman, 2004). Peat-based proxies include those
97 based on plant macrofossils, pollen, and testate amoebae (e.g., Woillard, 1978;
98 Mauquoy et al., 2008; Väiliranta et al., 2012), inorganic geochemistry (e.g., Burrows
99 et al., 2014; Chambers et al., 2014; Hansson et al., 2015; Vanneste et al., 2015), (bulk)
100 isotope signatures (e.g., Cristea et al., 2014; Roland et al., 2015) and organic
101 biomarkers (e.g., Nichols et al., 2006; Pancost et al., 2007; Pancost et al., 2011;
102 Huguet et al., 2014; Zocatelli et al., 2014; Schellekens et al., 2015; Zheng et al.,
103 2015). Although these proxies can be used to provide a detailed reconstruction of the
104 environment and biogeochemistry within the peat during deposition, an accurate
105 temperature or pH proxy for peat is currently lacking (Chambers et al., 2012). This is
106 particularly problematic because temperature and pH are key environmental
107 parameters that directly affect vegetation type, respiration rates, and a range of other
108 wetland features (e.g., Lafleur et al., 2005; Yvon-Durocher et al., 2014). The aim of
109 this paper is to develop peat-specific pH and temperature proxies for application to
110 peat cores as well as ancient peats from the geological record preserved as lignites.

111 We focus on using membrane-spanning glycerol dialkyl glycerol tetraether
112 (GDGT) lipids. In general, two types of GDGTs are abundant in natural archives such
113 as peats: 1) isoprenoidal (iso)GDGTs with *sn*-1 glycerol stereochemistry that are
114 synthesized by a wide range of Archaea, and 2) branched (br)GDGTs with *sn*-3
115 glycerol stereochemistry that are produced by Bacteria (see review by Schouten et al.,
116 2013 and references therein). A wide range of brGDGTs occur in natural archives
117 such as mineral soils and peat; specifically, tetra-, penta-, and hexamethylated
118 brGDGTs, each of which can contain 0, 1, or 2 cyclopentane rings (Weijers et al.,
119 2006b). In addition, recent studies using peat and mineral soils have demonstrated that
120 the additional methyl group(s) present in penta- and hexamethylated brGDGTs can

121 occur on either the α and/or ω -5 position (5-methyl brGDGTs) or the α and/or ω -6
122 position (6-methyl brGDGTs) (De Jonge et al., 2013; De Jonge et al., 2014).

123 brGDGTs are especially abundant in peat, in fact brGDGTs were first
124 discovered in a Dutch peat (Sinninghe Damsté et al., 2000). The concentration of
125 brGDGTs (as well as isoGDGTs) is much higher in the water saturated and
126 permanently anoxic catotelm of peat compared to the predominantly oxic acrotelm,
127 suggesting that brGDGTs are produced by anaerobic bacteria (Weijers et al., 2004;
128 Weijers et al., 2006a; Weijers et al., 2011), potentially members of the phylum
129 *Acidobacteria* (Weijers et al., 2009; Sinninghe Damsté et al., 2011; Sinninghe Damsté
130 et al., 2014). Although the exact source organism(s) are/is currently unknown, in
131 mineral soils (and potentially lakes) the distribution of bacterial brGDGTs is
132 correlated with mean annual air temperature (MAAT) and pH (Weijers et al., 2007;
133 Peterse et al., 2012; De Jonge et al., 2014; Loomis et al., 2014; Li et al., 2016). Over
134 the past decade ancient deposits of mineral soils (e.g., Peterse et al., 2014) and peat
135 (e.g., Ballantyne et al., 2010) have been used to reconstruct past terrestrial
136 temperatures.

137 Mineral soils differ from peat as the latter are normally water saturated,
138 consist predominantly of (partially decomposed) organic matter (the organic carbon
139 content of peat is typically > 30 wt.%), are typically acidic (pH 3-6), and have much
140 lower density. The combination of these factors means that peat becomes anoxic at
141 relatively shallow depths, whereas mineral soils are typically oxic. Indeed, Loomis et
142 al. (2011) showed that the brGDGT distribution in waterlogged soils is different from
143 that in dry soils and Dang et al. (2016) recently provided direct evidence of moisture
144 control on brGDGT distributions in soils. These differences suggest that microbial
145 lipids in peat might not reflect environmental variables, i.e. pH and temperature, in
146 the same way as they do in mineral soils.

147 Despite the high concentration of GDGTs in peats relatively few studies have
148 examined the environmental controls on their distribution in such settings (Huguet et
149 al., 2010; Weijers et al., 2011; Huguet et al., 2013; Zheng et al., 2015). Those studies
150 found that the application of soil-based proxies to peats can result in unrealistically
151 high temperature and pH estimates compared to the instrumental record. However,
152 owing to the small number of peats that have been studied to date as well as the lack
153 of peatland diversity sampled (the majority of peats sampled for these studies come
154 from temperate climates in Western Europe), the correlation of temperature and pH

155 with brGDGT distribution in peats is poorly constrained. Notably, the lack of tropical
156 peat brGDGT studies limits interpretations of brGDGT distributions in lignite
157 deposits from past greenhouse climates (Weijers et al., 2011).

158 Here we compare brGDGT distributions in a newly generated global data set
159 of peat with MAAT and (where available) *in situ* peat pH measurements. Our aim is
160 to gain an understanding of the impact of these environmental factors on the
161 distribution of brGDGTs in peat and develop for the first time peat-specific
162 temperature and pH proxies that can be used to reconstruct past terrestrial climate.

163

164 **2. Material and methods**

165 *2.1 Peat material*

166 We generated a collection of peat comprising a diverse range of samples from around
167 the world (Fig. 1). In total, our database consists of 470 samples from 96 different
168 peatlands. In order to assess the variation in brGDGT distribution within one location,
169 where possible we determined the brGDGT distribution in multiple horizons from
170 within the top 1m of peat (typically representing several centuries of accumulation)
171 and/or analyzed samples taken at slightly different places within the same peatland. A
172 peat deposit typically consists of an acrotelm and catotelm, although marked
173 heterogeneity can exist even over short distances (Baird et al., 2016). The acrotelm is
174 located above the water table for most of the year and characterized by oxic
175 conditions and active decomposition. The acrotelm overlies the catotelm, which is
176 permanently waterlogged and characterized by anoxic conditions and very slow
177 decomposition. Our dataset spans those biogeochemical gradients (e.g. acro/catotelm).
178 Variations in peat accumulation rates differ between sites, implying that the ages of
179 the brGDGT-pool might differ.

180 Our database includes peats from six continents and all major climate zones,
181 ranging from high latitude peats in Siberia, Canada, and Scandinavia to tropical peats
182 in Indonesia, Africa, and Peru (Fig. 2). It covers a broad range in MAAT from -8 to
183 27 °C. Although most samples come from acidic peats with pH <6, the dataset
184 includes several alkaline peats and overall our dataset spans a pH range from 3 to 8.
185 All samples come from freshwater peatlands, except for the one from the Shark River
186 peat (Everglades, USA) that is marine influenced. Unsurprisingly, given their global
187 distribution, the peats are characterized by a wide variety of vegetation, ranging from

188 *Sphagnum*-dominated ombrotrophic peats that are abundant in high-latitude and
189 temperate climates to (sub)tropical peats dominated by vegetation such as *Sagittaria*
190 (arrowhead) and *Cyperaceae* (sedge), and forested tropical peatlands.

191

192 2.2 Environmental parameters

193 The distribution of brGDGTs was compared to MAAT and *in situ* pH. MAAT was
194 obtained using the simple bioclimatic model PeatStash, which provides surface air
195 temperatures globally with a 0.5 degree spatial resolution (for details, see Kaplan et
196 al., 2003; Gallego-Sala and Prentice, 2013). The temperature data in PeatStash is
197 obtained by interpolating long-term mean weather station climatology (temperature,
198 precipitation and the fraction of possible sunshine hours) from around the world for
199 the period 1931–1960 (Climate 2.2 data are available online [http://www.pik-](http://www.pik-potsdam.de/~cramer/climate.html)
200 [potsdam.de/~cramer/climate.html](http://www.pik-potsdam.de/~cramer/climate.html)). Crucially, mean annual temperatures in peat are
201 similar to MAAT, assuming that the peat is not snow-covered for long periods of time
202 (McKenzie et al., 2007; Weijers et al., 2011). The temperature at the top surface of
203 (high-latitude) peat can differ from the MAAT due to insolation by snow during
204 winter and intense heating during summer. Despite this, the seasonal temperature
205 fluctuations in peat are dampened at depth as temperatures converge to MAAT
206 (Hillel, 1982; Laiho, 2006; McKenzie et al., 2007; Weijers et al., 2011). We assume
207 that all peat horizons experienced MAAT (the only data available on a global basis).
208 This is likely an oversimplification that introduces some additional uncertainty in our
209 calibration.

210 Where available, pH data were obtained from measured values reported in the
211 literature or our measurements during sampling. For peats, pH cannot be determined
212 using dried material, as is normally done for soils (Stanek, 1973). Accurate pH
213 measurements can only be obtained from *in situ* measurements, especially for
214 groundwater-fed wetlands, and these are not available for all locations.

215

216 2.3 Lipid extraction

217 For the majority of samples (>430 out of 470), between 0.1 and 0.5 g of dried bulk
218 peat were extracted with an Ethos Ex microwave extraction system with 20 mL of a
219 mixture of dichloromethane (DCM) and methanol (MeOH) (9:1, v/v) at the Organic
220 Geochemistry Unit (OGU) in Bristol. The microwave program consisted of a 10 min
221 ramp to 70 °C (1000 W), 10 min hold at 70 °C (1000 W), and 20 min cool down.

222 Samples were centrifuged at 1700 rounds per minute for 3 to 5 min and the
223 supernatant was removed and collected. 10 mL of DCM:MeOH (9:1) were added to
224 the remaining peat material and centrifuged again after which the supernatant was
225 removed and combined with the previously obtained supernatant. This process was
226 repeated 3 to 6 times, depending on the amount of extracted material, to ensure that
227 all extractable lipids were retrieved. The total lipid extract (TLE) was then
228 concentrated using rota-evaporation. An aliquot of the TLE (typically 25%) was
229 washed through a short (<2 cm) silica column using DCM:MeOH (9:1) to remove any
230 remaining peat particles. The TLE was dried under a gentle nitrogen flow and then re-
231 dissolved in hexane/*iso*-propanol (99:1, v/v) and filtered using 0.45 μm PTFE filters.

232 A small number of peats were extracted using different methods and either the
233 TLE or polar fraction was analyzed for GDGTs (see Table S1). Samples from the
234 Kyambanguru peat in Tanzania were extracted using the Bligh-Dyer protocol.
235 Previous work on peat demonstrated that the brGDGT distribution is similar using
236 Bligh-Dyer extraction as Soxhlet extraction (Chaves Torres and Pancost, 2016). The
237 TLE was cleaned over a short Si column at the OGU in Bristol. Both cleaned TLE
238 and polar fractions were re-dissolved in hexane/*iso*-propanol (99:1, v/v) and filtered
239 using 0.45 μm PTFE filters.

240

241 2.4 Analytical methods

242 All samples were analyzed for their core lipid GDGT distribution by high
243 performance liquid chromatography/atmospheric pressure chemical ionisation – mass
244 spectrometry (HPLC/APCI-MS) using a ThermoFisher Scientific Accela Quantum
245 Access triplequadrupole MS. Normal phase separation was achieved using two ultra-
246 high performance liquid chromatography silica columns, following Hopmans et al.
247 (2016). Crucially this method allows for the separation of the 5- and 6-methyl
248 brGDGT isomers. Injection volume was 15 μL , typically from 100 μL . Analyses were
249 performed using selective ion monitoring mode (SIM) to increase sensitivity and
250 reproducibility (m/z 1302, 1300, 1298, 1296, 1294, 1292, 1050, 1048, 1046, 1036,
251 1034, 1032, 1022, 1020, 1018, 744, and 653). The results were integrated manually
252 using the Xcalibur software. Based on daily measurements of an in-house generated
253 peat standard, analytical precession (σ) over the 12 months during which the data
254 were analyzed is 0.01 for the proxy index we define below ($\text{MBT}_{5\text{me}}$, eq. 2).

255

256 2.5 Proxy calculation

257 Guided by previous studies we used a range of proxies to express ratios of different

258 GDGTs and the nomenclature of De Jonge et al. (2014) (Fig. 1).

259

eq. (1) MBT

$$= \frac{(Ia + Ib + Ic)}{(Ia + Ib + Ic + IIa + IIa' + IIb + IIb' + IIc + IIc' + IIIa + IIIa' + IIIb + IIIb' + IIIc + IIIc')}$$

260 The original methylation of branched tetraether (MBT) index compared the relative
 261 abundance of tetramethylated brGDGTs (compounds Ia-Ic) to that of penta-
 262 (compounds IIa-IIc') and hexamethylated (compounds IIIa-IIIc') brGDGTs that have
 263 one or two additional methyl groups (Weijers et al., 2007). It was recently discovered
 264 that the additional methyl groups in penta- and hexamethylated brGDGTs can also
 265 occur at the C6 position (6-methyl brGDGTs, indicated by a prime symbol; e.g.
 266 brGDGT-IIa'): the 6-methyl penta- and hexamethylated brGDGTs (De Jonge et al.,
 267 2013). Excluding the 6-methyl brGDGTs from the MBT index resulted in the
 268 MBT_{5me'} index. In the global soil database the application of MBT_{5me'} led to an
 269 improved correlation with temperature (De Jonge et al., 2014).

$$eq. (2) MBT'_{5ME} = \frac{(Ia + Ib + Ic)}{(Ia + Ib + Ic + IIa + IIb + IIc + IIIa)}$$

270 In addition to different number of methyl groups, brGDGTs can contain up to two
 271 cyclopentane moieties (e.g., brGDGT-Ib and -Ic). CBT' is a modified version of the
 272 original cyclisation of branched tetraether (CBT) index (Weijers et al., 2007) and in
 273 soils CBT' has the best correlation with pH (De Jonge et al., 2014):

$$eq. (3) CBT' = \log \left(\frac{Ic + IIa' + IIb' + IIc' + IIIa' + IIIb' + IIIc'}{Ia + IIa + IIIa} \right)$$

274 The isomer ratio of 6-methyl brGDGTs (IR_{6me}) reflects the ratio between 5- and 6-
 275 methyl brGDGTs (Yang et al., 2015) with low (high) values indicative of a
 276 dominance of 5-methyl (6-methyl) brGDGTs:

$$eq. (4) IR_{6me} = \left(\frac{IIa' + IIb' + IIc' + IIIa' + IIIb' + IIIc'}{IIa + IIa' + IIb + IIb' + IIc + IIc' + IIIa + IIIa' + IIIb + IIIb' + IIIc + IIIc'} \right)$$

277

278 The isomerization of branched tetraethers (IBT) is related to IR_{6me} but reflects the

279 isomerization of brGDGT-IIa and -IIIa only (Ding et al., 2015):

$$\text{eq. (5) } IBT = -\log\left(\frac{IIa' + IIIa'}{IIa + IIIa}\right)$$

280 The branched versus isoprenoidal tetraether (BIT) index (Hopmans et al., 2004)
 281 reflects the relative abundance of the major bacterial brGDGTs versus a specific
 282 archaeal isoGDGT, crenarchaeol (Fig. 1), produced by *Thaumarchaeota* (Sinninghe
 283 Damsté et al., 2002):

$$\text{eq. (6) } BIT = \frac{Ia + IIa + IIa' + IIIa + IIIa'}{Ia + IIa + IIa' + IIIa + IIIa' + cren.}$$

284 Finally, the isoprenoidal over branched GDGT ratio ($R_{i/b}$), related to the BIT index,
 285 records the relative abundance of archaeal isoGDGTs over bacterial brGDGTs (Xie et
 286 al., 2012).

$$\text{eq. (7) } R_{i/b} = \frac{\sum isoGDGTs}{\sum brGDGTs}$$

287

288 2.6 Statistical methods

289 Temperature and pH calibrations were obtained using the average proxy value for
 290 each peat and Deming regressions. The software we used was RStudio
 291 (RStudio Team, 2015) and Method Comparison Regression (MCR) package
 292 (Manuilova et al., 2014), which are freely available to download¹. The Rscript and
 293 data are available in the appendices.

294 Deming regressions differ from simple linear regression, which so far have
 295 been used in brGDGT proxy calibrations, as they account for error in the data on both
 296 the x- (e.g., proxy) and y-axis (e.g., environmental variable) (Adcock, 1878).
 297 We used the average proxy value for each peat to calculate Deming regressions,
 298 calibration errors (RMSE, see below), and calibration coefficients of determination
 299 (R^2). The errors associated with proxy measurements (e.g. MBT_{5me}') and
 300 environmental parameters (MAAT/pH) are independent and assumed to be normally
 301 distributed. To calculate a Deming regression, the ratio of variances (δ) must be
 302 calculated. For MAAT we took a standard deviation (σ) of 1.5 °C based on the
 303 estimated mean predictive error of up to 1.4 °C for mean temperature in a similar
 304 dataset (New et al., 1999). For pH we took a standard deviation of 0.5 based on the
 305 average reported heterogeneity in pH for the peatlands used in the database (see
 306 Supplementary Table 1). For MBT_{5me}' , CBT' , and CBT_{peat} we calculated the average

¹ <https://www.rstudio.com> and <https://cran.r-project.org/web/packages/mcr/index.html>

307 standard deviation of each proxy from the entire peat data set (0.05, 0.25, and 0.2,
 308 respectively). This results in a ratio of variances of 0.0011 for the MBT_{5me}'/MAAT
 309 calibration and 0.25 and 0.16 for the pH calibration based on CBT' and CBT_{peat},
 310 respectively. Residuals were calculated for the full dataset and using

$$\text{eq. (8) } \text{Residual}_y = y_{\text{observed}} - y_{\text{predicted}}$$

311 The root mean square error (RMSE) for y , the predictive error for the
 312 environmental parameter of interest (MAAT or pH), was calculated for the average
 313 proxy value of each peat and using

$$\text{eq. (9) } \text{RSME}_y = \sqrt{\frac{\sum_{x=1}^n (y_{x,\text{observed}} - y_{x,\text{predicted}})^2}{n}} \times \frac{n}{df}$$

314 Where df stands for degrees of freedom, which in this case is $n-1$.

315

316 **3. Results**

317 Although we did not calculate concentrations, based on changes in signal intensity the
 318 relative abundance of GDGTs was always higher at depth compared to the top (~0–
 319 20) cm of peat. BIT indices (eq. 6) range between 0.75 and 1, but 99% of the samples
 320 have a BIT value ≥ 0.95 . Similarly, $R_{i/b}$ ratios are typically < 0.5 . Only three samples
 321 from the São João da Chapada peat in Brazil have a $R_{i/b}$ ratio > 1 .

322 The majority of brGDGTs are tetramethylated and 5-methyl penta- and
 323 hexamethylated brGDGTs. The most abundant brGDGTs in peat are brGDGT-Ia and
 324 IIa. By extension, the IR_{6me} ratio (eq. 4) is low. brGDGTs containing cyclopentane
 325 moieties are much less abundant than acyclic brGDGTs and brGDGT-IIIb(′) and -
 326 IIIc(′) are either below detection limit or present at trace abundances ($\leq 1\%$ of total
 327 brGDGTs). Indeed, three brGDGTs dominate the entire global dataset: tropical peats
 328 contain almost exclusively brGDGT-Ia (up to 99% of total brGDGTs), whereas in
 329 high-latitude peats brGDGT-IIa and -IIIa are dominant (Fig. 3).

330

331 **4. Discussion**

332 The observation that $R_{i/b}$ ratios are low in most peats is consistent with previous
 333 observations that bacterial brGDGTs dominate over archaeal isoprenoidal GDGTs in
 334 peat (Schouten et al., 2000; Sinninghe Damsté et al., 2000; Pancost et al., 2003) and
 335 mineral soils (Hopmans et al., 2004).

336

337 *4.1 Shallow vs deep GDGT distributions*

338 The apparent increase in GDGT abundance with depth is consistent with previous
339 observations in peatlands (Weijers et al., 2004; Peterse et al., 2011) and reflects the
340 combined effects of preferential GDGT production in anaerobic settings and the
341 accumulation of fossil GDGTs over time at depth (Liu et al., 2010; Weijers et al.,
342 2011).

343 In one high-latitude peat (Saxnäs Mosse, Sweden) the distribution of both
344 intact polar lipids (compounds still containing a polar head groups) and core
345 brGDGTs (compounds having lost their polar head group) differed between the acro-
346 and catotelm and brGDGT abundances were much higher in the latter (Weijers et al.,
347 2009; Peterse et al., 2011). Based on these results Peterse et al. (2011) speculated that
348 microbial communities differed between the oxic acrotelm and anoxic catotelm. As
349 oxygen content can influence cellular lipid composition of bacteria, Huguet et al.
350 (2010) speculated that oxygen availability could be one of the factors directly
351 influencing the brGDGT synthesis by bacteria in peat, as opposed to influencing the
352 type of source organism(s). Studies from lakes also suggested that changes in lake
353 oxygenation state can influence the brGDGT distribution (Tierney et al., 2012;
354 Loomis et al., 2014).

355 Our dataset consists of a mixture of surface (0–15 cm) and deeper samples
356 that extend through the top one meter of peat. For the majority of peats there is no
357 detailed information available on water table depths and location of the acro/catotelm
358 boundary. Nonetheless, to provide a first order assessment on whether there is a
359 systematic and significant difference in core brGDGT distribution between the upper
360 (assumed to be generally oxic) and underlying anoxic peat, we compared the relative
361 abundance of the three most abundant brGDGTs (Ia, IIa, and IIIa) in the shallow
362 surface peat (top 15 cm) with that of the deep peat below 15 cm (Fig. 3), although we
363 acknowledge that this is likely an oversimplification.

364 There are some differences. In general the relative abundance of brGDGT-Ia
365 is slightly higher in the top 15 cm of a peat compared to the peat below 15 cm,
366 especially when its abundance is < 60%. Overall, however, the distributions plot
367 along the 1:1 line, indicating that there is no systematic difference in brGDGT
368 distribution between the (assumed) oxic surface and the peat below 15 cm (likely
369 anoxic). This does not preclude differences in brGDGT production between oxic and
370 anoxic conditions, but this appears to be primarily expressed via greater production of

371 brGDGTs under anoxic conditions as demonstrated by the higher abundance of
372 GDGTs across the acro/catotelm boundary (Weijers et al., 2006a). These results
373 provide indirect evidence that oxygen availability does not significantly impact the
374 degree of methylation of (core) brGDGTs. One possible explanation for why oxygen
375 availability does not affect distributions is that brGDGTs could be predominantly
376 produced by anaerobes throughout the peat, in low abundance in anaerobic
377 microenvironments in shallow peat and in high abundance in the anaerobic catotelm.

378 Several (high-latitude) peats, however, do appear to exhibit strong variations
379 between deep and shallow sections of the peat. The down core records from Stordalen
380 (Sweden) and Andorra (S. Patagonia), for example, are characterized by a large and
381 abrupt shift in brGDGT distribution at depth (Fig. 4). The MBT_{5me}' indices recorded
382 at the very top of these high-latitude peats are between 0.8 and 0.6, as high as those
383 found in mid-latitude and subtropical peats, but decrease to values between 0.2 and
384 0.4 below ~30 cm. Peats from temperate climates (e.g. Walton moss, UK) and the
385 tropics (e.g. Sebangau, Indonesia) display much smaller or no change in brGDGT
386 distribution with depth (Fig. 4 and 5). It appears that this offset in brGDGT
387 distribution with depth is amplified in high-latitude peats. This is consistent with
388 previous studies that indicated a difference in brGDGT-distribution between the acro-
389 and catotelm in a high-latitude peat from southern Sweden (Weijers et al., 2009;
390 Peterse et al., 2011).

391 We argue that the high MBT_{5me}' values at the top of these high-latitude peats
392 are heavily biased towards summer temperatures. At these settings winter
393 temperatures are often below freezing for a prolonged period, likely causing bacterial
394 growth and GDGT production to slow down significantly. Summer temperatures are
395 much higher (e.g. mean warmest month temperature at Stordalen is around 13 °C), in-
396 line with the observed relatively high MBT_{5me}' values (e.g., 0.6-0.7 at Stordalen, see
397 Figure 4). Deeper in the peat, seasonal temperature fluctuations are much less
398 pronounced and temperatures rapidly converge to the MAAT (Vitt et al., 1995; Laiho,
399 2006; McKenzie et al., 2007; Weijers et al., 2011), likely accounting for the lower
400 MBT_{5me}' values in the deeper peat horizons. Moreover, the greater production of
401 GDGTs in the anaerobic part of the peat will cause GDGT-based temperatures to
402 rapidly converge on the deep peat growth temperature, overprinting the seasonal
403 summer bias of fossil GDGTs synthesized at the surface.

404 This effect is diminished in temperate and especially tropical peatlands from
405 around sea level, which we attribute to the lack of a preferred growing season in
406 settings with smaller seasonal temperature ranges. In such settings temperatures are
407 less frequently (or never) below freezing and brGDGT production in the top of the
408 peat likely occurs for all or most of the year, such that GDGTs produced in both the
409 shallow and deeper part of the peat record MAAT. This hypothesis needs further
410 testing but indicates that 1) brGDGT production may be biased towards the warm
411 season in the upper part of high-latitude/altitude peats; 2) care has to be taken when
412 interpreting brGDGT-based trends in the top of such peats; and 3) the temperature
413 signal in such peats is imparted at depth, such that downcore GDGT variations in
414 ancient peat archives could potentially be temporally offset (precede) the climate
415 events that caused them. However, as brGDGTs in long peat cores, and by extension
416 ancient lignites (fossilized peats), are dominated by production at depth where
417 temperature equals MAAT (see section 2.2) it is very unlikely that temperatures
418 obtained from these archives are seasonally biased.

419 In the remainder of this work, for high-latitude peats that show a clear offset
420 between the top and deeper part of the peat we use only the average GDGT
421 distribution from below 20 cm, as the majority of change appears to occur in the top
422 20 cm. For the other peats we retain all data from the upper 1 m, not differentiating
423 between the acro- and catotelm. To generate the temperature and pH calibrations we
424 use the average brGDGT distribution for each peatland. For peats where multiple
425 samples were analyzed, error bars indicate the deviation (1σ) from the average.

426

427 *4.2 Influence of temperature and pH on brGDGTs in peats*

428 It is well established that in soils and lakes, environmental conditions such as
429 temperature and pH are highly correlated with the brGDGT distribution (e.g., Weijers
430 et al., 2007; Peterse et al., 2012; Schoon et al., 2013; De Jonge et al., 2014; Loomis et
431 al., 2014; Xiao et al., 2015; Li et al., 2016). In the following sections we investigate
432 the influence of these parameters on the brGDGT distribution in peat using the
433 average proxy value (e.g. MBT_{5me}') for each peatland.

434

435 *4.2.1 Influence of peat pH on brGDGT distribution*

436 Weijers et al. (2007) demonstrated that in a global mineral soil database the degree of
437 cyclisation of brGDGTs is correlated to pH, with a higher fractional abundance of

438 brGDGTs that contain cyclopentane moieties in soils with a higher pH. Following the
439 discovery of 6-methyl brGDGTs (De Jonge et al., 2013), it was shown that the degree
440 of isomerization of brGDGTs, the ratio of 6-methyl versus 5-methyl brGDGTs, is also
441 correlated to soil pH, with a higher fractional abundance of 6-methyl brGDGTs in
442 soils with a higher pH (De Jonge et al., 2014; Xiao et al., 2015). Owing to the limited
443 pH range of the few peats used to study brGDGTs so far and because all of these
444 studies pre-date the recent analytical advances that allow for the separation of 5- and
445 6-methyl brGDGTs, it is unknown whether pH has an influence on brGDGTs in peats
446 or whether the dependence is similar to that found in soils. Our peat database spans a
447 pH range from 3 to 8, similar to that of the soil database, allowing us to assess the
448 influence of pH on the brGDGT distribution in such settings.

449 Although pH measurements are only available in 51 out of 96 peats, our
450 results indicate that 6-methyl brGDGTs are present at either only trace abundances
451 ($IR_{6me} < 0.1$) or are absent in acidic peats with $pH < 5.4$ (Fig 6). Higher ratios occur in
452 peats with higher pH. The highest ratio (0.58) occurs in the marine-influenced
453 alkaline peat from the Everglades. Not surprisingly, the fractional abundances of the
454 three most common 6-methyl brGDGTs (brGDGT-IIa', -IIb', -IIIa') are significantly
455 correlated with pH with R-values between 0.4 and 0.6 ($p < 0.01$) (Fig. 7). These results
456 are consistent with observations from soils that indicate a positive correlation between
457 the fractional abundance of 6-methyl brGDGTs and pH (De Jonge et al., 2014; Xiao
458 et al., 2015).

459 As a result, the IR_{6me} as well as the related IBT index, both of which have
460 been used to reconstruct pH in soils (Ding et al., 2015; Xiao et al., 2015), are
461 correlated with pH in the peats (not shown). However, this comparison is complicated
462 by the fact that 6-methyl brGDGTs are absent in many of the peats. For IR_{6me} the
463 absence of 6-methyl brGDGTs results in values that are 0, whereas IBT cannot be
464 calculated for samples that lack 6-methyl brGDGTs as the logarithm of zero is
465 undefined.

466 The abundance of 6-methyl brGDGTs is generally lower in peats than in
467 mineral soils with comparable pH. Indeed, 6-methyl brGDGTs are present in 99% of
468 all soils in the global soil database, including soils with $pH < 5$ where IR_{6me} ratios can
469 be as high as 0.4 (Fig. 6). Recent work has shown that in addition to pH the fractional
470 abundance of 6-methyl brGDGTs is negatively correlated with soil water content,
471 with fewer 6-methyl brGDGTs versus 5-methyl brGDGTs in soils with 60% water

472 content compared to soils with < 10% water content (Dang et al., 2016). It is likely
 473 that the negative correlation between soil water content and fractional abundance of 6-
 474 methyl brGDGTs can explain the overall lower IR_{6me} in peats as these are generally
 475 water saturated.

476 In addition to 6-methyl brGDGTs, the fractional abundances of brGDGTs
 477 containing cyclopentane moieties (brGDGT-Ib and -IIb) are also significantly
 478 correlated to pH ($R = 0.73$ and 0.56 , $p < 0.01$, respectively) (Fig. 7a and 7c). The other
 479 brGDGTs are not significantly correlated to pH. These observations are consistent
 480 with those from soils, where both 5- and 6-methyl brGDGTs containing cyclopentane
 481 moieties are more abundant at higher pH (Weijers et al., 2007; Peterse et al., 2012; De
 482 Jonge et al., 2014). Consequently, and similar to soils (De Jonge et al., 2014; Xiao et
 483 al., 2015), CBT' (eq. 3) in peat can be modeled as a function of pH (Fig. 8):

$$\text{eq. (10) } pH = 2.69 \times CBT' + 9.19 \quad (n = 50, R^2 = 0.44, \text{RMSE} = 1.0)$$

484 The slope of this calibration is different (higher) from that found in soils (see
 485 supplementary information), but the coefficient of determination is lower, and the
 486 RMSE is higher. A stronger correlation is obtained by using only compounds that are
 487 significantly correlated to pH in the numerator, CBT_{peat}:

$$\text{eq. (11) } CBT_{peat} = \log \left(\frac{Ib + IIa' + IIb + IIb' + IIIa'}{Ia + IIa + IIIa} \right)$$

$$\text{eq. (12) } pH = 2.49 \times CBT_{peat} + 8.07 \quad (n = 51, R^2 = 0.58, \text{RMSE} = 0.8)$$

488 Although the coefficient of determination increases and RMSE decreases using
 489 CBT_{peat}, the calibration uncertainties are still larger than those reported for soils (see
 490 supplementary information).

491 It is noteworthy that in peats the correlation between brGDGT distributions
 492 and pH is much weaker than that with MAAT (see below). This contrasts with
 493 mineral soils, for which the correlation of CBT' with pH ($R^2 = 0.85$), is stronger than
 494 that of MAT_{mr} with MAAT ($R^2 = 0.68$) (De Jonge et al., 2014). The weaker
 495 correlation can partly be explained by the smaller sample set used for the peat
 496 calibration ($n = 51$) versus soil calibration ($n = 221$),. However, taking 51 random
 497 mineral soils from the latter still yields a stronger correlation between CBT' and pH
 498 than we obtain for the peat data set. In addition, the coefficient of determination of a
 499 calibration based only on peats with $pH \geq 5$ is ~ 0.5 for CBT_{peat}, similar to that of the
 500 complete data set. We argue that the difference could be related to the observation
 501 that in mineral soils water content also influences the brGDGT distribution, especially

502 that of 6-methyl brGDGTs (e.g., Menges et al., 2014). Recently Dang et al. (2016)
 503 showed that $CBT_{(5me)}$ is higher in dry soils compared to wet soils. Because alkaline
 504 soils are often also dry whereas acidic soils are often wet, this effect could enhance
 505 the correlation between CBT' and pH in soils. As peats are typically water saturated,
 506 the additional effect of soil water content is lacking, which may explain the weaker
 507 correlation between CBT' and pH in peats compared to mineral soils.

508

509 4.2.2 Influence of MAAT on brGDGTs in peats

510 In mineral soils the distribution of brGDGTs is influenced by MAAT, with the degree
 511 of methylation decreasing as temperature increases (Weijers et al., 2007; De Jonge et
 512 al., 2014). A temperature effect on the brGDGT distribution was recently also found
 513 in one peatland (Huguet et al., 2013). Although the producers of brGDGTs are
 514 currently unknown, such a response is consistent with homeoviscous adaptation
 515 (Weijers et al., 2007). Here we investigate whether temperature has a significant
 516 correlation with brGDGTs in peats on a global scale.

517 When plotted against MAAT, only 5-methyl brGDGTs lacking cyclopentane
 518 moieties (brGDGT-Ia, -IIa, and -IIIa) have significant correlations with MAAT (Fig.
 519 9). brGDGT-Ia is positively correlated with MAAT ($R = 0.72$, $p < 0.01$), whereas
 520 brGDGT-IIa ($R = 0.82$, $p < 0.01$), and -IIIa ($R = 0.63$, $p < 0.01$) are negatively correlated
 521 with MAAT. These correlations are significantly higher than those found in the global
 522 soil data set (De Jonge et al., 2014). The degree of methylation of 5-methyl brGDGTs
 523 is captured in the MBT_{5me}' index (eq. 2). As such we use the MBT_{5me}' index to
 524 construct a peat-specific temperature proxy (Fig. 10):

$$\text{eq. (13) } MAAT_{peat} (\text{°C}) = 52.18 \times MBT'_{5me} - 23.05 \quad (n = 96, R^2 = 0.76, \text{RMSE} \\ = 4.7 \text{ °C})$$

525 Crucially, no correlation is observed between MBT_{5me}' and pH ($R^2 = 0$ and $p > 0.8$)
 526 and we observe no trend in the residuals. The coefficient of determination (R^2) of
 527 $MAAT_{peat}$ is higher compared to a Deming regression of the expanded soil dataset (R^2
 528 $= 0.60$, see supplementary information) as well as that of the linear MBT_{5me}'
 529 calibration ($R^2 = 0.66$) suggested by De Jonge et al. (2014). Crucially, because the
 530 slope of the $MAAT_{peat}$ calibration is steeper, it could have greater utility for the
 531 reconstruction of tropical temperatures ($MAAT_{peat}$ reaches saturation at 29.1 °C),
 532 although these maximum temperatures are higher than the maximum MAAT in the

533 modern calibration data set which is 26.7 °C. In contrast, the Deming MBT_{5me}' soil
534 calibration reaches saturation (i.e. MBT_{5me}' = 1) at a temperature of 24.8 °C (see
535 supplementary information), while the linear MBT_{5me}' calibration suggested by De
536 Jonge et al. (2014) has a maximum of 22.9 °C.

537

538 *4.3 Implications for paleoclimate reconstructions and future work*

539 Compared to the natural archives previously used to reconstruct past terrestrial
540 temperature change (e.g., riverine, lacustrine, and marine sediments), peats have a
541 major advantage. For example, the brGDGTs in peat are mainly derived from *in situ*
542 production. Mixing of brGDGT source areas, which complicates the application of
543 GDGTs in sediments that represent a large catchment area (e.g., Zell et al., 2014; De
544 Jonge et al., 2015; Sinninghe Damsté, 2016), is unlikely to be a problem. In addition,
545 peats are overall characterized by anoxic conditions and the preservation potential of
546 organic compounds such as brGDGTs is high. Finally, as peats are water saturated,
547 especially the catotelm where the majority of brGDGT production occurs, the
548 additional influence of changes in moisture content (Menges et al., 2014; Dang et al.,
549 2016) is also negligible. Nevertheless, there are limitations to this proxy that need to
550 be considered when evaluating suitable palaeoclimate applications, and we explore
551 those below.

552

553 *4.3.1 Late Holocene climate*

554 Here we provide peat-specific temperature and pH proxies that could be used to
555 reconstruct terrestrial climate over a broad range of time scales, including the late
556 Holocene. However, the estimated variation in terrestrial temperature of most places
557 on earth during the last millennium is typically less than 1°C (Mann et al., 2009;
558 Pages 2k Consortium, 2013), although there could be local exceptions. Such
559 temperature change is much smaller than the calibration error (RMSE of ~ 4.7 °C).
560 Although based on different lipids produced by different organisms, GDGT proxies
561 can potentially record temperature changes smaller than the calibration errors when
562 utilized within a highly constrained site-specific study (Tierney et al., 2010), although
563 this interpretation was recently contested (Kraemer et al., 2015).

564 Regardless of calibration issues, application of the MAAT_{peat} calibration to
565 late Holocene palaeoclimate remains problematic. A potential seasonal bias in the top
566 of some high-latitude peats, as well as a potential difference between oxic and anoxic

567 production, appear to prevent application of this proxy to shallow peat sediments.
568 Indeed, our downcore profiles spanning the top 1 meter of peat exhibit changes in
569 brGDGT distributions equivalent to temperature variations of up to several degrees
570 Celsius, larger than the expected climate variations. Moreover, as discussed above,
571 GDGTs appear to be predominantly generated at depth, and although this evidently
572 ensures they record MAAT it does mean that their reconstructed temperature signals
573 start in deeper peat horizons, i.e. stratigraphically preceding the climate changes that
574 caused them.

575 Future work should determine whether these peat-specific proxies can be used
576 to reconstruct small amplitude and/or short-lived temperature variation. However we
577 currently urge caution in applying the peat-specific proxies to shallow peat cores to
578 reconstruct late Holocene climate (e.g., Little Ice Age or Medieval Warm anomaly).
579

580 *4.3.2 Application to the last glacial*

581 We envision these proxies are well-suited to reconstruct large amplitude and more
582 long-term temperature excursions such as those associated with the last glacial
583 termination and early Holocene. Such transitions are recorded in some particularly
584 long peat cores at several places around the world (e.g., McGlone et al., 2010;
585 Vanneste et al., 2015; Zheng et al., 2015; Baker et al., 2016). To test whether the
586 novel peat-specific temperature calibration can be used to reconstruct
587 glacial/interglacial temperature variability, we applied this proxy to samples from the
588 Hani peat sequence (Fig. 2). Hani peat is located in northeastern China and in places
589 is up to 10 meters thick, spanning ~16,000 cal yrs (Zhou et al., 2010). We analyzed
590 two samples from ~840 cm depth (corresponding to the late glacial at around 15.3
591 kyr), and compared MAAT_{peat} with that of two samples from around 100 cm depth
592 (corresponding to the late Holocene with an age of 700-1000 yrs). Using MAAT_{peat}
593 we obtained an average temperature of around -0.8 °C for the late glacial (15.3 kyr).
594 For the late Holocene (0.7-1 kyr) we obtained an average temperature of around 4.6
595 °C (Table 1).

596 Taking the calibration error of ~4.7 °C into account the reconstructed late
597 Holocene temperatures (4.6 °C) are close to the observed modern-day MAAT of
598 around 4 °C at this locality (Zhou et al., 2010). In contrast, applying soil calibrations
599 to reconstruct MAAT at this site results in significantly higher values (up to 11 °C;
600 Table 1). MAAT_{peat} (as well as the soil MBT_{5me'} calibration) indicates that

601 temperatures increased from the late glacial to the late Holocene by around 5 °C. In
602 contrast the MAT_{mr} mineral soil calibration indicates a smaller increase of around 3
603 °C. A ~ 5 °C increase is similar to that observed in east Asian loess-paleosol
604 sequences (Peterse et al., 2014), although that is based on the MBT(°)/CBT method.
605 In addition a 5 °C deglacial temperature increase is similar to those of several sea
606 surface temperature records available from similar latitudes in the Sea of Japan (Lee,
607 2007). The next step should be multiproxy temperature reconstructions in a variety of
608 locations to test the new calibration and to determine whether absolute temperatures
609 obtained using MAAT_{peat} are reliable. Nonetheless, this initial analysis indicates that
610 MAAT_{peat} yields temperature estimates that are consistent with both modern day
611 observations and other proxy estimates for the last glacial.

612

613 *4.3.3 Deep time application*

614 We see considerable scope for future work with this proxy to reconstruct terrestrial
615 temperature during past greenhouse periods and across hyperthermals (e.g
616 Paleocene/Eocene Thermal Maximum; PETM). These events are recorded in lignite
617 deposits. For example the PETM is documented in lignites from the UK (Collinson et
618 al., 2003; Pancost et al., 2007). Importantly, lignites are the lowest (maturity) rank of
619 coal and have not experienced significant burial and associated temperature and
620 pressure that leads to the loss of GDGTs (Schouten et al., 2004, 2013). Due to their
621 low thermal maturity, lignites are thought to retain their original brGDGT distribution
622 over geological timescales. For example, brGDGTs have been reported in an
623 immature late Paleocene lignite from the USA (Weijers et al., 2011), early Eocene
624 lignites from Germany (Inglis et al., 2017), as well as Miocene lignite from Germany
625 (Stock et al., 2016). Although analyzed using the classical analytical method that did
626 not separate 5 and 6-methyl brGDGTs, the brGDGT distribution in a late Paleocene
627 lignite from North America is dominated by brGDGT-Ia (Weijers et al., 2011),
628 similar to that seen in modern peats from the tropics and suggesting high terrestrial
629 temperatures. This is consistent with our overall understanding of terrestrial climate
630 during the greenhouse world of the late Paleocene and early Eocene (Huber and
631 Caballero, 2011).

632 As the brGDGT distribution in peat deposits is dominated by production in the
633 anoxic catotelm below the water table where the seasonal temperature cycle is muted
634 (see section 4.1) brGDGT-based temperatures obtained from lignite deposits can be

635 considered to reflect MAAT. We envision that future studies applying our new peat-
636 specific calibrations to immature lignites will provide valuable new insights into
637 terrestrial climate during the geological past. In addition, the GDGT concentrations in
638 peats are generally much higher than those found in soils. We therefore propose that
639 for studies of brGDGT distributions in (marine) sediments with a peat-dominated
640 catchment area (e.g. Siberia (Frey and Smith, 2005)) or that contain independent
641 evidence for the input of peat-derived material (e.g. high concentration of $C_{31} \alpha\beta$ -
642 hopanes or palynologic evidence for the input of typical peatland vegetation), the
643 majority of GDGTs is likely derived from peatlands. In such settings it is more
644 appropriate to use a peat-specific calibration rather than a mineral soil calibration.

645

646 **5. Conclusions**

647 Using 470 samples from 96 peatlands from around the world we explored the
648 environmental controls on the bacterial brGDGT distribution in peats. We
649 demonstrate that brGDGT distributions are correlated with peat pH and especially
650 mean annual air temperature (MAAT). We develop for the first time peat-specific
651 brGDGT-derived pH and temperature calibrations. In addition to their application in
652 ancient peat-forming environments, we also suggest that these calibrations could be
653 preferable to the available mineral soil calibration in marginal marine settings when it
654 is clear that brGDGTs are predominantly derived from peats. We suggest caution in
655 applying this proxy to late Holocene peat (e.g., covering the Medieval Climatic
656 Anomaly and/or Little Ice Age) as both the calibration error and downcore variation
657 appears to be larger than expected climate signals during this period. Taken together
658 our results demonstrate that there is clear potential to use GDGTs in peatlands and
659 lignites to reconstruct past terrestrial climate, opening up a new set of sedimentary
660 archives that will help to improve understanding of the climate system during the
661 geological past.

662

663 **Acknowledgements**

664 This research was funded through the advanced ERC grant “the greenhouse earth
665 system” (T-GRES, project reference 340923), awarded to RDP. All authors are part of
666 the “T-GRES Peat Database collaborators” collective. RDP also acknowledges the
667 Royal Society Wolfson Research Merit Award. We thank D. Atkinson for help with
668 the sample preparation. We acknowledge support from Labex VOLTAIRE (ANR-10-

669 LABX-100-01). Peat from Patagonia and Tierra del Fuego were collected thanks to a
 670 Young Researcher Grant of the Agence National de la Recherche (ANR) to FDV,
 671 project ANR-2011-JS56-006-01 “PARAD” and with the help of Ramiro Lopez,
 672 Andrea Coronato and Veronica Pancotto (CADIC-CONICET, Ushuaia). Peat from
 673 Brazil was collected with the context of CNPq project 482815/2011-6. Samples from
 674 France (Frasne and La Guette) were collected thanks to the French Observatory of
 675 Peatlands. The Canadian peat was collected in the context of the NSERC-Discovery
 676 grant of L. Rochefort. Peats from China were obtained under a National Natural
 677 Science Foundation of China grant (No. 41372033), awarded to Y. Zheng. We thank
 678 the editor, 3 anonymous reviewers, and Jess Tierney for valuable comments.

679

680 **References:**

- 681 Adcock, R.J., 1878. A Problem in Least Squares. *Analyst* **5** (2), 53-54.
 682
 683 Baird, A.J., Milner, A.M., Blundell, A., Swindles, G.T., Morris, P.J., 2016.
 684 Microform-scale variations in peatland permeability and their ecohydrological
 685 implications. *J. Ecol.* **104** (2), 531-544.
 686
 687 Baker, A., Routh, J., Roychoudhury, A.N., 2016. Biomarker records of
 688 palaeoenvironmental variations in subtropical Southern Africa since the late
 689 Pleistocene: Evidences from a coastal peatland. *Palaeogeogr. Palaeoclimatol.*
 690 *Palaeoecol.* **451**, 1-12.
 691
 692 Ballantyne, A.P., Greenwood, D.R., Sinninghe Damsté, J.S., Csank, A.Z., Eberle, J.J.,
 693 Rychczynski, N., 2010. Significantly warmer Arctic surface temperatures during the
 694 Pliocene indicated by multiple independent proxies. *Geology* **38** (7), 603-606.
 695
 696 Barber, K.E., 1993. Peatlands as scientific archives of past biodiversity. *Biodivers.*
 697 *Conserv.* **2** (5), 474-489.
 698
 699 Burrows, M.A., Fenner, J., Haberle, S.G., 2014. Humification in northeast Australia:
 700 Dating millennial and centennial scale climate variability in the late Holocene.
 701 *Holocene* **24** (12), 1707-1718.
 702
 703 Chambers, F.M., Charman, D.J., 2004. Holocene environmental change: contributions
 704 from the peatland archive. *Holocene* **14** (1), 1-6.
 705
 706 Chambers, F.M., Booth, R.K., De Vleeschouwer, F., Lamentowicz, M., Le Roux, G.,
 707 Mauquoy, D., Nichols, J.E., et al., 2012. Development and refinement of proxy-
 708 climate indicators from peats. *Quatern. Int.* **268**, 21-33.
 709
 710 Chambers, F.M., Brain, S.A., Mauquoy, D., McCarroll, J., Daley, T., 2014. The
 711 ‘Little Ice Age’ in the Southern Hemisphere in the context of the last 3000 years:
 712 Peat-based proxy-climate data from Tierra del Fuego. *Holocene* **24** (12), 1649-1656.

- 713
714 Chaves Torres, L., Pancost, R.D., 2016. Insoluble prokaryotic membrane lipids in a
715 *Sphagnum* peat: Implications for organic matter preservation. *Org. Geochem.* **93**, 77-
716 91.
717
- 718 Collinson, M.E., Hooker, J.J., Gröcke, D.R., 2003. Cobham Lignite Bed and
719 penecontemporaneous macrofloras of southern England: A record of vegetation and
720 fire across the Paleocene-Eocene Thermal Maximum, in: Wing, S.L., Gingerich, P.D.,
721 Schmitz, B., Thomas, B. (Eds.), Causes and Consequences of Globally Warm
722 Climates in the Early Paleogene. Geological Society of America, Boulder, Colorado,
723 pp. 333-349.
724
- 725 Cristea, G., Cuna, S.M., Fărcaș, S., Tanțău, I., Dordai, E., Măgdaș, D.A., 2014.
726 Carbon isotope composition as an indicator of climatic changes during the middle and
727 late Holocene in a peat bog from the Maramureș Mountains (Romania). *Holocene* **24**,
728 15-23.
729
- 730 Dang, X., Yang, H., Naafs, B.D.A., Pancost, R.D., Evershed, R.P., Xie, S., 2016.
731 Direct evidence of moisture control on the methylation of branched glycerol dialkyl
732 glycerol tetraethers in semi-arid and arid soils. *Geochim. Cosmochim. Acta* **189**, 24-
733 36.
734
- 735 De Jonge, C., Hopmans, E.C., Stadnitskaia, A., Rijpstra, W.I.C., Hofland, R.,
736 Tegelaar, E., Sinninghe Damsté, J.S., 2013. Identification of novel penta- and
737 hexamethylated branched glycerol dialkyl glycerol tetraethers in peat using HPLC-
738 MS², GC-MS and GC-SMB-MS. *Org. Geochem.* **54**, 78-82.
739
- 740 De Jonge, C., Hopmans, E.C., Zell, C.I., Kim, J.-H., Schouten, S., Sinninghe Damsté,
741 J.S., 2014. Occurrence and abundance of 6-methyl branched glycerol dialkyl glycerol
742 tetraethers in soils: implications for palaeoclimate reconstruction. *Geochim.*
743 *Cosmochim. Acta* **141**, 97-112.
744
- 745 De Jonge, C., Stadnitskaia, A., Hopmans, E.C., Cherkashov, G., Fedotov, A.,
746 Streletskaia, I.D., Vasiliev, A.A., et al., 2015. Drastic changes in the distribution of
747 branched tetraether lipids in suspended matter and sediments from the Yenisei River
748 and Kara Sea (Siberia): Implications for the use of brGDGT-based proxies in coastal
749 marine sediments. *Geochim. Cosmochim. Acta* **165**, 200-225.
750
- 751 Ding, S., Xu, Y., Wang, Y., He, Y., Hou, J., Chen, L., He, J.S., 2015. Distribution of
752 branched glycerol dialkyl glycerol tetraethers in surface soils of the Qinghai-Tibetan
753 Plateau: implications of brGDGTs-based proxies in cold and dry regions.
754 *Biogeosciences* **12** (11), 3141-3151.
755
- 756 Frey, K.E., Smith, L.C., 2005. Amplified carbon release from vast West Siberian
757 peatlands by 2100. *Geophys. Res. Lett.* **32** (9), L09401.
758
- 759 Gallego-Sala, A.V., Prentice, C.I., 2013. Blanket peat biome endangered by climate
760 change. *Nat. Clim. Chang.* **3** (2), 152-155.
761

- 762 Gorham, E., Janssens, J.A., Glaser, P.H., 2003. Rates of peat accumulation during the
763 postglacial period in 32 sites from Alaska to Newfoundland, with special emphasis on
764 northern Minnesota. *Can. J. Bot.* **81** (5), 429-438.
- 765
766 Hansson, S.V., Bindler, R., De Vleeschouwer, F., 2015. Using Peat Records as
767 Natural Archives of Past Atmospheric Metal Deposition, in: Blais, J.M., Rosen, M.R.,
768 Smol, J.P. (Eds.), *Environmental Contaminants*. Springer Netherlands, pp. 323-354.
- 769
770 Hillel, D., 1982. *Introduction to Soil Physics*. Academic Press, New York.
- 771
772 Hopmans, E.C., Weijers, J.W.H., Schefuß, E., Herfort, L., Sinninghe Damsté, J.S.,
773 Schouten, S., 2004. A novel proxy for terrestrial organic matter in sediments based on
774 branched and isoprenoid tetraether lipids. *Earth Plant. Sc. Lett.* **224** (1-2), 107-116.
- 775
776 Hopmans, E.C., Schouten, S., Sinninghe Damsté, J.S., 2016. The effect of improved
777 chromatography on GDGT-based palaeoproxies. *Org. Geochem.* **93**, 1-6.
- 778
779 Huber, M., Caballero, R., 2011. The early Eocene equable climate problem revisited.
780 *Clim. Past* **7** (2), 603-633.
- 781
782 Huguet, A., Fosse, C., Laggoun-Défarge, F., Toussaint, M.-L., Derenne, S., 2010.
783 Occurrence and distribution of glycerol dialkyl glycerol tetraethers in a French peat
784 bog. *Org. Geochem.* **41** (6), 559-572.
- 785
786 Huguet, A., Fosse, C., Laggoun-Défarge, F., Delarue, F., Derenne, S., 2013. Effects of
787 a short-term experimental microclimate warming on the abundance and distribution of
788 branched GDGTs in a French peatland. *Geochim. Cosmochim. Acta* **105**, 294-315.
- 789
790 Huguet, A., Francez, A.-J., Jusselme, M.D., Fosse, C., Derenne, S., 2014. A climatic
791 chamber experiment to test the short term effect of increasing temperature on
792 branched GDGT distribution in *Sphagnum* peat. *Org. Geochem.* **73**, 109-112.
- 793
794 Inglis, G.N., Collinson, M.E., Riegel, W., Wilde, V., Farnsworth, A., Lunt, D.J.,
795 Valdes, P., et al., 2017. Mid-latitude continental temperatures through the early
796 Eocene in western Europe. *Earth Plant. Sc. Lett.* **460**, 86-96.
- 797
798 Kaplan, J.O., Bigelow, N.H., Prentice, I.C., Harrison, S.P., Bartlein, P.J., Christensen,
799 T.R., Cramer, W., et al., 2003. Climate change and Arctic ecosystems: 2. Modeling,
800 paleodata-model comparisons, and future projections. *J. Geophys. Res.-Atmos.* **108**
801 (D19).
- 802
803 Kraemer, B.M., Hook, S., Huttula, T., Kotilainen, P., O'Reilly, C.M., Peltonen, A.,
804 Plisnier, P.-D., et al., 2015. Century-Long Warming Trends in the Upper Water
805 Column of Lake Tanganyika. *PLOS ONE* **10** (7), e0132490.
- 806
807 Lafleur, P.M., Moore, T.R., Roulet, N.T., Frohking, S., 2005. Ecosystem Respiration
808 in a Cool Temperate Bog Depends on Peat Temperature But Not Water Table.
809 *Ecosystems* **8** (6), 619-629.
- 810

- 811 Laiho, R., 2006. Decomposition in peatlands: Reconciling seemingly contrasting
812 results on the impacts of lowered water levels. *Soil Biol. Biochem.* **38** (8), 2011-2024.
813
- 814 Lee, K.E., 2007. Surface water changes recorded in Late Quaternary marine
815 sediments of the Ulleung Basin, East Sea (Japan Sea). *Palaeogeogr. Palaeoclimatol.*
816 *Palaeoecol.* **247** (1–2), 18-31.
817
- 818 Lei, Y., Yang, H., Dang, X., Zhao, S., Xie, S., 2016. Absence of a significant bias
819 towards summer temperature in branched tetraether-based paleothermometer at two
820 soil sites with contrasting temperature seasonality. *Org. Geochem.* **94**, 83-94.
821
- 822 Li, J., Pancost, R.D., Naafs, B.D.A., Yang, H., Zhao, C., Xie, S., 2016. Distribution of
823 glycerol dialkyl glycerol tetraether (GDGT) lipids in a hypersaline lake system. **99**,
824 113-124.
825
- 826 Liu, X.-L., Leider, A., Gillespie, A., Gröger, J., Versteegh, G.J.M., Hinrichs, K.-U.,
827 2010. Identification of polar lipid precursors of the ubiquitous branched GDGT
828 orphan lipids in a peat bog in Northern Germany. *Org. Geochem.* **41** (7), 653-660.
829
- 830 Loomis, S.E., Russell, J.M., Sinninghe Damsté, J.S., 2011. Distributions of branched
831 GDGTs in soils and lake sediments from western Uganda: Implications for a
832 lacustrine paleothermometer. *Org. Geochem.* **42** (7), 739-751.
833
- 834 Loomis, S.E., Russell, J.M., Eggermont, H., Verschuren, D., Sinninghe Damsté, J.S.,
835 2014. Effects of temperature, pH and nutrient concentration on branched GDGT
836 distributions in East African lakes: Implications for paleoenvironmental
837 reconstruction. *Org. Geochem.* **66**, 25-37.
838
- 839 Mann, M.E., Zhang, Z., Rutherford, S., Bradley, R.S., Hughes, M.K., Shindell, D.,
840 Ammann, C., et al., 2009. Global Signatures and Dynamical Origins of the Little Ice
841 Age and Medieval Climate Anomaly. *Science* **326** (5957), 1256-1260.
842
- 843 Manuilova, E., Schuetzenmeister, A., Model, F., 2014. Method Comparison
844 Regression. CRAN, <https://cran.r-project.org/web/packages/mcr/index.html>.
845
- 846 Mauquoy, D., Yeloff, D., Van Geel, B., Charman, D.J., Blundell, A., 2008. Two
847 decadal resolved records from north-west European peat bogs show rapid climate
848 changes associated with solar variability during the mid-late Holocene. *J. Quat. Sci.*
849 **23** (8), 745-763.
850
- 851 McGlone, M.S., Turney, C.S.M., Wilmshurst, J.M., Renwick, J., Pahnke, K., 2010.
852 Divergent trends in land and ocean temperature in the Southern Ocean over the past
853 18,000 years. *Nat. Geosci.* **3** (9), 622-626.
854
- 855 McKenzie, J.M., Siegel, D.I., Rosenberry, D.O., Glaser, P.H., Voss, C.I., 2007. Heat
856 transport in the Red Lake Bog, Glacial Lake Agassiz Peatlands. *Hydrol. Process.* **21**
857 (3), 369-378.
858
- 859 Menges, J., Huguet, C., Alcañiz, J.M., Fietz, S., Sachse, D., Rosell-Melé, A., 2014.
860 Influence of water availability in the distributions of branched glycerol dialkyl

- 861 glycerol tetraether in soils of the Iberian Peninsula. *Biogeosciences* **11** (10), 2571-
862 2581.
- 863
- 864 New, M., Hulme, M., Jones, P., 1999. Representing Twentieth-Century Space–Time
865 Climate Variability. Part I: Development of a 1961–90 Mean Monthly Terrestrial
866 Climatology. *J. Climate* **12** (3), 829-856.
- 867
- 868 Nichols, J.E., Booth, R.K., Jackson, S.T., Pendall, E.G., Huang, Y., 2006.
869 Paleohydrologic reconstruction based on *n*-alkane distributions in ombrotrophic peat.
870 *Org. Geochem.* **37** (11), 1505-1513.
- 871
- 872 Pages 2k Consortium, 2013. Continental-scale temperature variability during the past
873 two millennia. *Nat. Geosci.* **6** (5), 339-346.
- 874
- 875 Pancost, R.D., Baas, M., van Geel, B., Sinninghe Damsté, J.S., 2003. Response of an
876 ombrotrophic bog to a regional climate event revealed by macrofossil, molecular and
877 carbon isotopic data. *Holocene* **13** (6), 921-932.
- 878
- 879 Pancost, R.D., Steart, D.S., Handley, L., Collinson, M.E., Hooker, J.J., Scott, A.C.,
880 Grassineau, N.V., et al., 2007. Increased terrestrial methane cycling at the Palaeocene-
881 Eocene thermal maximum. *Nature* **449** (7160), 332-335.
- 882
- 883 Pancost, R.D., McClymont, E.L., Bingham, E.M., Roberts, Z., Charman, D.J.,
884 Hornibrook, E.R.C., Blundell, A., et al., 2011. Archaeol as a methanogen biomarker
885 in ombrotrophic bogs. *Org. Geochem.* **42** (10), 1279-1287.
- 886
- 887 Peterse, F., Hopmans, E.C., Schouten, S., Mets, A., Rijpstra, W.I.C., Sinninghe
888 Damsté, J.S., 2011. Identification and distribution of intact polar branched tetraether
889 lipids in peat and soil. *Org. Geochem.* **42** (9), 1007-1015.
- 890
- 891 Peterse, F., van der Meer, J., Schouten, S., Weijers, J.W.H., Fierer, N., Jackson, R.B.,
892 Kim, J.-H., et al., 2012. Revised calibration of the MBT–CBT paleotemperature proxy
893 based on branched tetraether membrane lipids in surface soils. *Geochim. Cosmochim.*
894 *Acta* **96**, 215-229.
- 895
- 896 Peterse, F., Martínez-García, A., Zhou, B., Beets, C.J., Prins, M.A., Zheng, H.,
897 Eglinton, T.I., 2014. Molecular records of continental air temperature and monsoon
898 precipitation variability in East Asia spanning the past 130,000 years. *Quaternary Sci.*
899 *Rev.* **83**, 76-82.
- 900
- 901 Roland, T.P., Daley, T.J., Caseldine, C.J., Charman, D.J., Turney, C.S.M., Amesbury,
902 M.J., Thompson, G.J., et al., 2015. The 5.2 ka climate event: Evidence from stable
903 isotope and multi-proxy palaeoecological peatland records in Ireland. *Quat. Sci. Rev.*
904 **124**, 209-223.
- 905
- 906 RStudio Team, 2015. RStudio: Integrated Development for R. RStudio, Inc., Boston,
907 MA (USA).
- 908
- 909 Schellekens, J., Bindler, R., Martínez-Cortizas, A., McClymont, E.L., Abbott, G.D.,
910 Biester, H., Pontevedra-Pombal, X., et al., 2015. Preferential degradation of

- 911 polyphenols from *Sphagnum* – 4-Isopropenylphenol as a proxy for past hydrological
912 conditions in *Sphagnum*-dominated peat. *Geochim. Cosmochim. Acta* **150**, 74-89.
913
- 914 Schoon, P.L., de Kluijver, A., Middelburg, J.J., Downing, J.A., Sinninghe Damsté,
915 J.S., Schouten, S., 2013. Influence of lake water pH and alkalinity on the distribution
916 of core and intact polar branched glycerol dialkyl glycerol tetraethers (GDGTs) in
917 lakes. *Org. Geochem.* **60**, 72-82.
918
- 919 Schouten, S., Hopmans, E.C., Pancost, R.D., Sinninghe Damsté, J.S., 2000.
920 Widespread occurrence of structurally diverse tetraether membrane lipids: Evidence
921 for the ubiquitous presence of low-temperature relatives of hyperthermophiles. *Proc.*
922 *Natl. Acad. Sci.* **97** (26), 14421-14426.
923
- 924 Schouten, S., Hopmans, E.C., Sinninghe Damsté, J.S., 2004. The effect of maturity
925 and depositional redox conditions on archaeal tetraether lipid palaeothermometry.
926 *Org. Geochem.* **35** (5), 567-571.
927
- 928 Schouten, S., Hopmans, E.C., Sinninghe Damsté, J.S., 2013. The organic
929 geochemistry of glycerol dialkyl glycerol tetraether lipids: A review. *Org. Geochem.*
930 **54**, 19-61.
931
- 932 Sinninghe Damsté, J.S., Hopmans, E.C., Pancost, R.D., Schouten, S., Geenevasen,
933 J.A.J., 2000. Newly discovered non-isoprenoid glycerol dialkyl glycerol tetraether
934 lipids in sediments. *Chem. Commun.*(17), 1683-1684.
935
- 936 Sinninghe Damsté, J.S., Schouten, S., Hopmans, E.C., van Duin, A.C.T., Geenevasen,
937 J.A.J., 2002. Crenarchaeol: the characteristic core glycerol dibiphytanyl glycerol
938 tetraether membrane lipid of cosmopolitan pelagic crenarchaeota. *J. Lipid. Res.* **43**
939 (10), 1641-1651.
940
- 941 Sinninghe Damsté, J.S., Rijpstra, W.I.C., Hopmans, E.C., Weijers, J.W.H., Foessel,
942 B.U., Overmann, J., Dedysh, S.N., 2011. 13,16-Dimethyl Octacosanedioic Acid (*iso*-
943 Diabolic Acid), a Common Membrane-Spanning Lipid of *Acidobacteria* Subdivisions
944 1 and 3. *Appl. Environ. Microb.* **77** (12), 4147-4154.
945
- 946 Sinninghe Damsté, J.S., Rijpstra, W.I.C., Hopmans, E.C., Foessel, B.U., Wüst, P.K.,
947 Overmann, J., Tank, M., et al., 2014. Ether- and Ester-Bound *iso*-Diabolic Acid and
948 Other Lipids in Members of *Acidobacteria* Subdivision 4. *Appl. Environ. Microb.* **80**
949 (17), 5207-5218.
950
- 951 Sinninghe Damsté, J.S., 2016. Spatial heterogeneity of sources of branched tetraethers
952 in shelf systems: The geochemistry of tetraethers in the Berau River delta
953 (Kalimantan, Indonesia). *Geochim. Cosmochim. Acta* **186**, 13-31.
954
- 955 Stanek, W., 1973. Comparisons of methods of pH determination for organic terrain
956 surveys. *Can. J. Soil Sci.* **53** (2), 177-183.
957
- 958 Stock, A.T., Littke, R., Lücke, A., Zieger, L., Thielemann, T., 2016. Miocene
959 depositional environment and climate in western Europe: The lignite deposits of the
960 Lower Rhine Basin, Germany. *Int. J. Coal. Geol.* **157**, 2-18.

- 961
962 Tierney, J.E., Mayes, M.T., Meyer, N., Johnson, C., Swarzenski, P.W., Cohen, A.S.,
963 Russell, J.M., 2010. Late-twentieth-century warming in Lake Tanganyika
964 unprecedented since AD 500. *Nat. Geosci.* **3** (6), 422-425.
965
- 966 Tierney, J.E., Schouten, S., Pitcher, A., Hopmans, E.C., Sinninghe Damsté, J.S.,
967 2012. Core and intact polar glycerol dialkyl glycerol tetraethers (GDGTs) in Sand
968 Pond, Warwick, Rhode Island (USA): Insights into the origin of lacustrine GDGTs.
969 *Geochim. Cosmochim. Acta* **77**, 561-581.
970
- 971 Väiliranta, M., Blundell, A., Charman, D.J., Karofeld, E., Korhola, A., Sillasoo, Ü.,
972 Tuittila, E.S., 2012. Reconstructing peatland water tables using transfer functions for
973 plant macrofossils and testate amoebae: A methodological comparison. *Quat. Int.* **268**,
974 34-43.
975
- 976 Vanneste, H., De Vleeschouwer, F., Martínez-Cortizas, A., von Scheffer, C.,
977 Piotrowska, N., Coronato, A., Le Roux, G., 2015. Late-glacial elevated dust
978 deposition linked to westerly wind shifts in southern South America. *Sci. Rep.* **5**,
979 11670
980
- 981 Vitt, D.H., Bayley, S.E., Jin, T.-L., 1995. Seasonal variation in water chemistry over a
982 bog-rich fen gradient in Continental Western Canada. *Can. J. Fish. Aquat. Sci.* **52** (3),
983 587-606.
984
- 985 Weijers, J.W.H., Schouten, S., van der Linden, M., van Geel, B., Sinninghe Damsté,
986 J.S., 2004. Water table related variations in the abundance of intact archaeal
987 membrane lipids in a Swedish peat bog. *FEMS Microbiol. Lett.* **239** (1), 51-56.
988
- 989 Weijers, J.W.H., Schouten, S., Hopmans, E.C., Geenevasen, J.A.J., David, O.R.P.,
990 Coleman, J.M., Pancost, R.D., et al., 2006a. Membrane lipids of mesophilic anaerobic
991 bacteria thriving in peats have typical archaeal traits. *Environ. Microbiol.* **8** (4), 648-
992 657.
993
- 994 Weijers, J.W.H., Schouten, S., Spaargaren, O.C., Sinninghe Damsté, J.S., 2006b.
995 Occurrence and distribution of tetraether membrane lipids in soils: Implications for
996 the use of the TEX₈₆ proxy and the BIT index. *Org. Geochem.* **37** (12), 1680-1693.
997
- 998 Weijers, J.W.H., Schouten, S., van den Donker, J.C., Hopmans, E.C., Sinninghe
999 Damsté, J.S., 2007. Environmental controls on bacterial tetraether membrane lipid
1000 distribution in soils. *Geochim. Cosmochim. Acta* **71** (3), 703-713.
1001
- 1002 Weijers, J.W.H., Panoto, E., van Bleijswijk, J., Schouten, S., Rijpstra, W.I.C., Balk,
1003 M., Stams, A.J.M., et al., 2009. Constraints on the Biological Source(s) of the Orphan
1004 Branched Tetraether Membrane Lipids. *Geomicrobiol. J.* **26** (6), 402-414.
1005
- 1006 Weijers, J.W.H., Steinmann, P., Hopmans, E.C., Schouten, S., Sinninghe Damsté,
1007 J.S., 2011. Bacterial tetraether membrane lipids in peat and coal: Testing the MBT-
1008 CBT temperature proxy for climate reconstruction. *Org. Geochem.* **42** (5), 477-486.
1009

- 1010 Woillard, G.M., 1978. Grande Pile peat bog: A continuous pollen record for the last
1011 140,000 years. *Quaternary Res.* **9** (1), 1-21.
1012
- 1013 Xiao, W., Xu, Y., Ding, S., Wang, Y., Zhang, X., Yang, H., Wang, G., et al., 2015.
1014 Global calibration of a novel, branched GDGT-based soil pH proxy. *Org. Geochem.*
1015 **89–90**, 56-60.
1016
- 1017 Xie, S., Pancost, R.D., Chen, L., Evershed, R.P., Yang, H., Zhang, K., Huang, J., et
1018 al., 2012. Microbial lipid records of highly alkaline deposits and enhanced aridity
1019 associated with significant uplift of the Tibetan Plateau in the Late Miocene. *Geology*
1020 **40** (4), 291-294.
1021
- 1022 Yang, H., Lü, X., Ding, W., Lei, Y., Dang, X., Xie, S., 2015. The 6-methyl branched
1023 tetraethers significantly affect the performance of the methylation index (MBT) in
1024 soils from an altitudinal transect at Mount Shennongjia. *Org. Geochem.* **82**, 42-53.
1025
- 1026 Yvon-Durocher, G., Allen, A.P., Bastviken, D., Conrad, R., Gudasz, C., St-Pierre, A.,
1027 Thanh-Duc, N., et al., 2014. Methane fluxes show consistent temperature dependence
1028 across microbial to ecosystem scales. *Nature* **507** (7493), 488-491.
1029
- 1030 Zell, C., Kim, J.H., Balsinha, M., Dorhout, D., Fernandes, C., Baas, M., Sinninghe
1031 Damsté, J.S., 2014. Transport of branched tetraether lipids from the Tagus River basin
1032 to the coastal ocean of the Portuguese margin: consequences for the interpretation of
1033 the MBT/CBT paleothermometer. *Biogeosciences* **11** (19), 5637-5655.
1034
- 1035 Zheng, Y., Li, Q., Wang, Z., Naafs, B.D.A., Yu, X., Pancost, R.D., 2015. Peatland
1036 GDGT records of Holocene climatic and biogeochemical responses to the Asian
1037 Monsoon. *Org. Geochem.* **87**, 86-95.
1038
- 1039 Zhou, W., Zheng, Y., Meyers, P.A., Jull, A.J.T., Xie, S., 2010. Postglacial climate-
1040 change record in biomarker lipid compositions of the Hani peat sequence,
1041 Northeastern China. *Earth Planet. Sc. Lett.* **294** (1–2), 37-46.
1042
- 1043 Zocatelli, R., Jacob, J., Gogo, S., Le Milbeau, C., Rousseau, J., Laggoun-Défarge, F.,
1044 2014. Spatial variability of soil lipids reflects vegetation cover in a French peatland.
1045 *Org. Geochem.* **76**, 173-183.
1046

1047 **Figure captions**

1049 Fig. 1: Structures of brGDGTs (with numbering) as well as isoprenoidal GDGT
1050 crenarchaeol (cren), following (De Jonge et al., 2014). Roman numbers indicate tetra-
1051 (I), penta- (II), and hexamethylated (III) brGDGTs, whereas letters indicate the
1052 absence (a), presence of one (b), or two (c) cyclopentane rings. Prime symbols
1053 indicate 6-methyl brGDGTs in which the additional methyl groups of the penta- and
1054 hexamethylated brGDGTs occur at the α and/or ω -6 position instead of α and/or ω -5
1055 position of 5-methyl brGDGTs.

1056

1057 Fig. 2: Map with the location of all peats used in this study. The star indicates the
1058 location of the Hani peat sequence in NE China.

1059

1060 Fig. 3: Fractional abundances of the three main brGDGTs in the top 15 cm of each
1061 peat (assumed to be representative of the oxic acrotelm) versus the fractional
1062 abundance of these brGDGTs between 15 and 100 cm in the peat (assumed to be
1063 representative for the anoxic catotelm). For peats where multiple samples were
1064 analyzed, error bars represent 1σ from the average fractional abundance.

1065

1066 Fig. 4: Down core record of MBT_{5me}' in four peats: a high-latitude peat from Sweden
1067 (blue squares), high-latitude peat from Patagonia (orange squares), temperate peat
1068 from the UK (green triangles), and tropical peat from Indonesia (purple diamonds).
1069 (For interpretation of the references to color in this figure legend, the reader is
1070 referred to the web version of this article.)

1071

1072 Fig. 5: Standard deviation of MBT_{5me}' for each low-altitude (< 1000 m) peat versus
1073 latitude. The four peats used in figure 4 are highlighted.

1074

1075 Figure 6: Ratio of 6-methyl over 5-methyl brGDGTs (IR_{6me}) versus pH for peat
1076 samples (black squares) together with the IR_{6me} in the top 10 cm of mineral soils
1077 (orange circles) (De Jonge et al., 2014; Ding et al., 2015; Xiao et al., 2015; Yang et
1078 al., 2015; Lei et al., 2016). Vertical error bars on the peat data represent 1σ and are
1079 based on the analysis of multiple horizons from the same peat. Horizontal error bars
1080 represent the spread in pH reported for each peat. (For interpretation of the references
1081 to color in this figure legend, the reader is referred to the web version of this article.)

1082

1083 Figure 7: Fractional abundance of brGDGT versus pH for those compounds with a r-
1084 value greater than 0.45 A) brGDGT-Ib, B) brGDGT-IIa', C) brGDGT-IIb, D)
1085 brGDGT-IIb', and E) brGDGT-IIIa' ($p < 0.01$ for all compounds). Samples with
1086 fractional abundances < 0.001 are not included. Vertical error bars represent 1σ and
1087 are based on the analysis of multiple horizons from the same peat. Horizontal error
1088 bars represent the spread in pH reported for each peat.

1089

1090 Fig. 8: A) Average CBT' for each peat versus pH (black circles) and C) average
1091 CBT_{peat} for each peat versus pH (black circles). Solid blue lines in A and C represent
1092 the Deming regression used to obtain the calibrations, while dashed black lines reflect
1093 simple linear regressions. Horizontal error bars represent 1σ and are based on the
1094 analysis of horizons samples from the same peat. Vertical error bars represent the
1095 spread in pH reported for each peat. Also shown is the residual pH for all analyzed
1096 peat samples (yellow circles), obtained by subtracting the estimated pH using the
1097 CBT' (B) and CBT_{peat} (D) deming calibrations from the observed pH. (For
1098 interpretation of the references to color in this figure legend, the reader is referred to
1099 the web version of this article.)

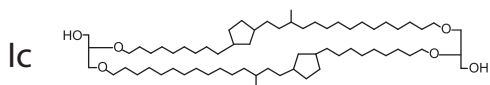
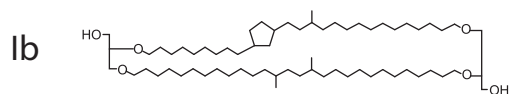
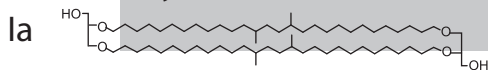
1100

1101 Fig. 9: Fractional abundance of the three main brGDGT versus MAAT A) brGDGT-
1102 Ia, B) brGDGT-IIa, and C) brGDGT-IIIa ($p < 0.01$ for all compounds). Samples with
1103 fractional abundances < 0.001 were not included. Vertical error bars represent 1σ and
1104 are based on the analysis of multiple horizons from the same peat.

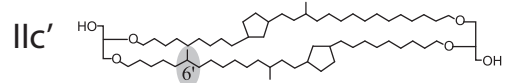
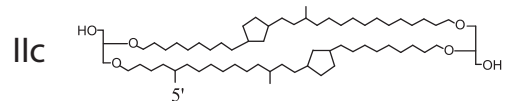
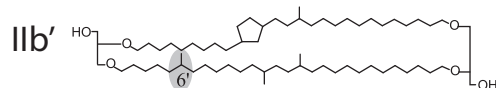
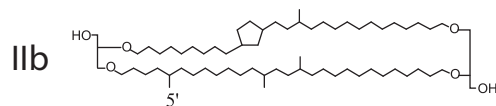
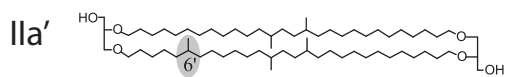
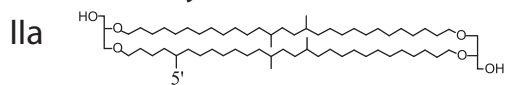
1105

1106 Fig. 10: Average MBT_{5me}' for each peat versus MAAT (black circles). The solid blue
1107 line represents the Deming regression, whereas dashed lines reflect the simple linear
1108 regression. Horizontal error bars represent 1σ and are based on the analysis of
1109 multiple horizons from the same peat. Also shown is the residual MAAT of all
1110 analyzed peat samples (yellow circles) obtained by subtracting the estimated MAAT
1111 using the MBT_{5me}' Deming calibration from the observed MAAT. (For interpretation
1112 of the references to color in this figure legend, the reader is referred to the web
1113 version of this article).

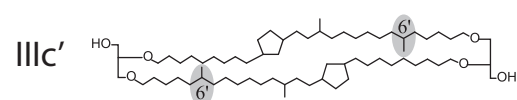
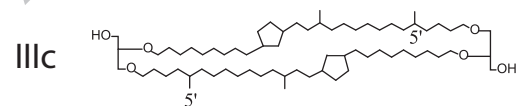
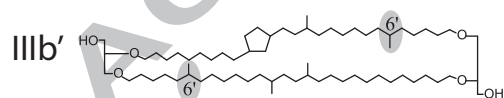
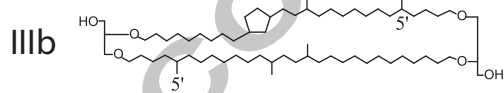
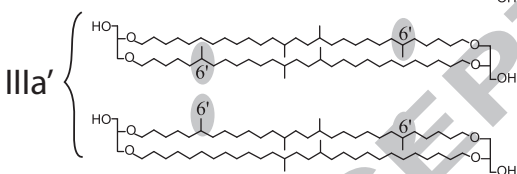
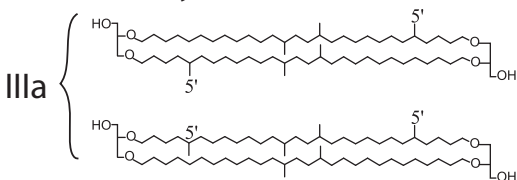
Depth (cm)	Age (yr)	MBT _{5ME'}	MAT _{mr} soil (RMSE 4.6 °C)	MAT _{5me'} soil (RMSE 4.8 °C)	MAAT _{peat} (RMSE 4.7 °C)
			De Jonge, 2014	De Jonge, 2014	This study
86	~700	0.53	6.6	10.9	4.5
102	~1000	0.53	6.6	11.3	4.8
838	~15,100	0.46	4.4	6.7	1.2
846	~15,400	0.39	2.8	5.4	-2.7
		Δ MAAT	3.0 °C	5.0 °C	5.4 °C



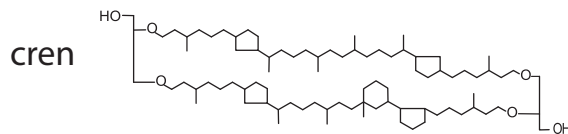
Pentamethylated brGDGTs

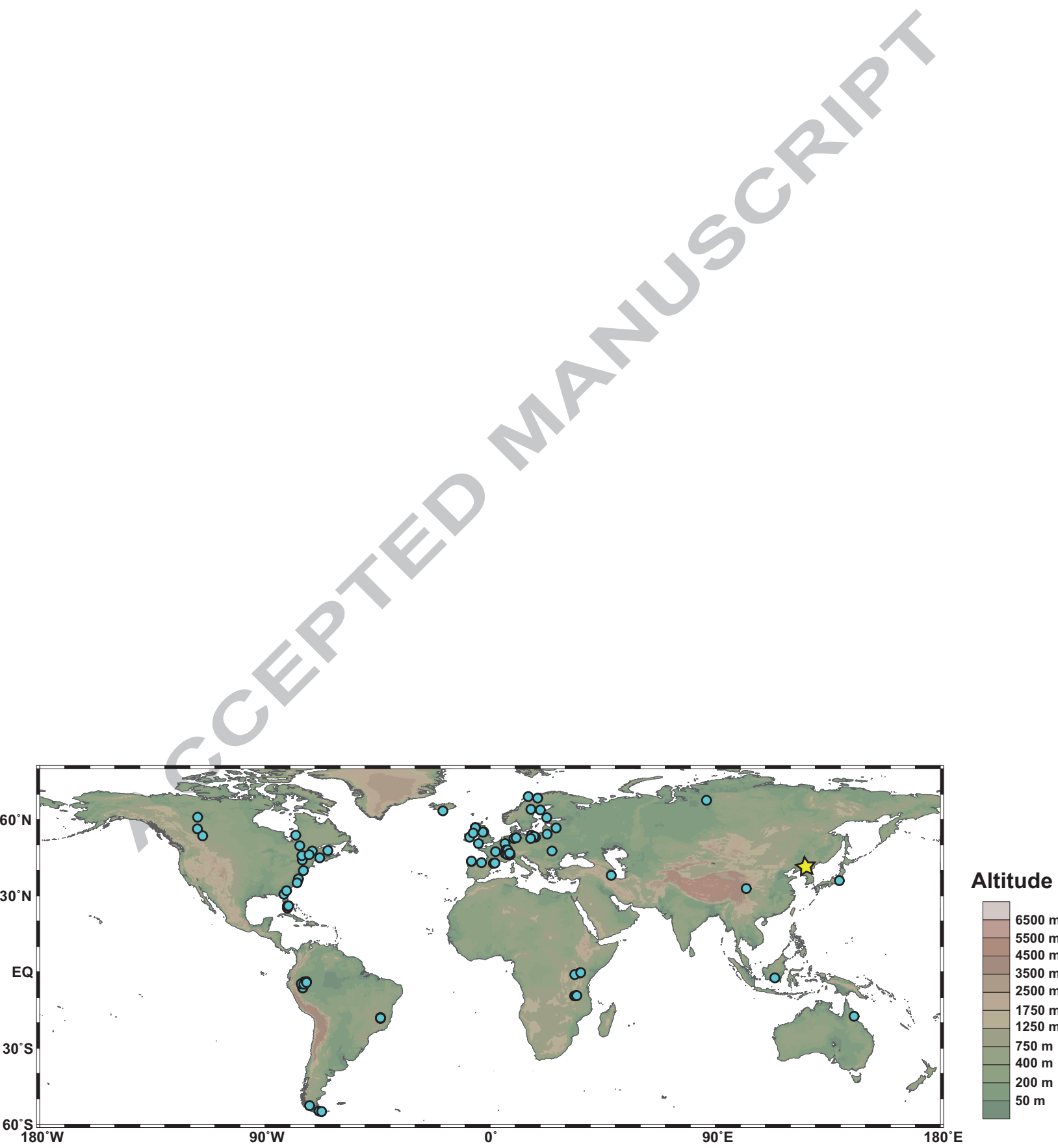


Hexamethylated brGDGTs



Crenarchaeol





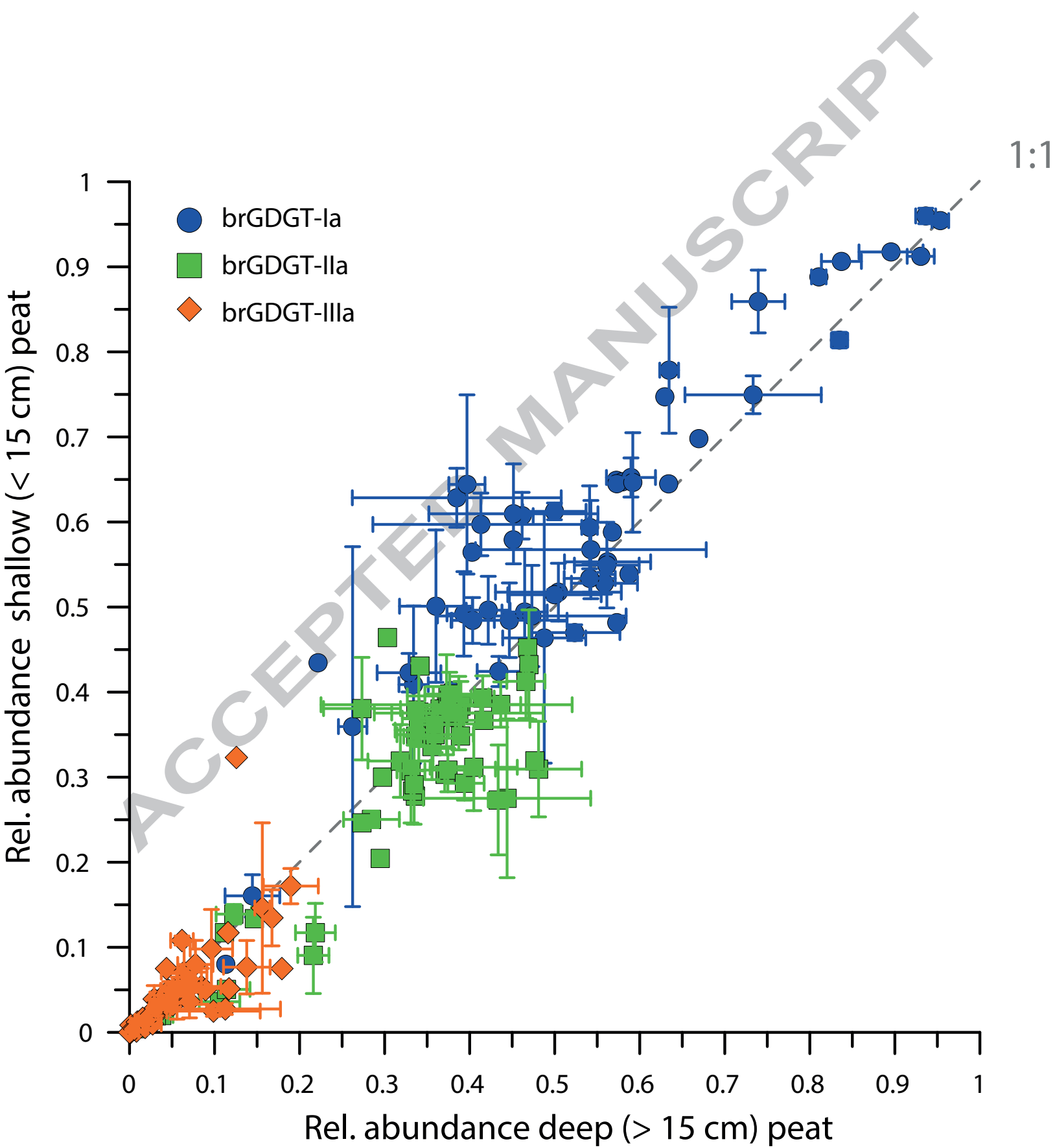


Figure 4

